INTERNATIONAL JOURNAL OF OPTIMIZATION IN CIVIL ENGINEERING
Int. J. Optim. Civil Eng., 2023; 13(4):413-438

A HYBRID SIMULATED ANNEALING, PARTICLE SWARM AND ANT COLONY OPTIMIZATION FOR DESIGN OF DOUBLE-CURVED DAMS

M. Shahrouzi[*, †] , S.-Sh. Emamzadeh and Y. Naserifar
Civil Engineering Department, Faculty of Engineering, Kharazmi University, Tehran, Iran

[DOI: 10.22068/ijoce.2023.13.4.564]

ABSTRACT

Shape optimization of a double-curved dam is formulated using control points for interpolation functions. Every design vector is decoded into the integrated water-dam-foundation rock model. An enhanced algorithm is proposed by hybridizing particle swarm algorithm with ant colony optimization and simulated annealing. The best experiences of the search agents are indirectly shared via pheromone trail deposited on a bi-partite characteristic graph. Such a stochastic search is further tuned by Boltzmann functions in simulated annealing. The proposed method earned the first rank in comparison with six well-known meta-heuristic algorithms in solving benchmark test functions. It captured the optimal shape design of Morrow Point dam, as a widely addressed case-study, by 21% reduced concrete volume with respect to the common USBR design practice and 16% better than the particle swarm optimizer. Such an optimal design was also superior to the others in stress redistribution for better performance of the dam system.

Keywords: Double-curved dam; Concrete infrastructure; Shape Optimization; Particle Swarm Optimization; Graph Theory; Ant Colony Optimization; Simulated Annealing

Received: 12 April 2023; Accepted: 11 June 2023

1. INTRODUCTION

Design of a concrete dam is one of the real-world problems that bring about high economic impact. Concrete volume as the main construction material plays a major role in the total

[*]Corresponding author: Civil Engineering Department, Faculty of Engineering, Kharazmi University, Tehran & Karaj, Iran
[†]E-mail address: shahruzi@khu.ac.ir (Mohsen Shahrouzi)

cost of such an infrastructure. Therefore, its minimization has been already addressed as a rewarding task by several investigators [1–3]. The optimization methods seek for the best design to find the optimal shape of the dam provided that it can successfully withstand natural loads.

Sharma [4] utilizes the theory of plates and shells to seek for the best design of dam with a repetitive trial and error method. Sharpe [5] treated shape and geometry optimization of a concrete dam by Sequential Linear Programming (SQP) as a branch of MP. Wassermann [6] used a mathematical formulation utilizing some shape functions and consequently employed SQP to solve the optimization problem. Yao and Choi [1] applied higher-order elements for the structural analysis in the design of dams. Some research works between 1987 and 1992 introduced a practical continuous geometrical model for shape optimization of the double-curved dams [7].

An alternative solution is to apply zero-order stochastic methods that do not require any gradient calculations (despite traditional MP) for optimal design. These methods include meta-heuristic algorithms as a branch of stochastic search with the capability of escaping from local optima toward global optimum. Some methods in this category can be referred to as Ant Colony Optimization (ACO) [8], Simulated Annealing (SA)[9], Harmony Search (HS) [10], Genetic Algorithm (GA) [11], Particle Swarm Optimization (PSO) [12], Water Evaporation Optimization (WEO) [13], Falcon Optimization Algorithm (FOA) [14], Atom Search Optimization (ASO) [15], Aquila Optimizer (AO) [16], Escaping Bird Search (EBS) [17] and Artificial Hummingbird Algorithm (AHA) [18], among several others.

PSO is a pioneer method of swarm intelligence with simple moving strategies that makes it a scalable easy-to-use and general-purpose algorithm [19]. It has already been hybridized with some other methods for performance improvement. Liu et al. [20] hybridized PSO with Differential Evolution (DE) [21]. Hadidi et al. [22] utilized a strategy for search refinement about the global best of PSO regarding normal distribution and simulated annealing. Hassani et al. [23] employed a hybrid PSO with Ant Lion Optimizer (ALO) [24] for optimization of various test functions and 7 real-world benchmarks.

In addition to such attempts for optimization of trusses and other engineering benchmarks, a number of studies have addressed optimal design of dams. They include the application of GA in shape optimization of dams [25, 26]. Kaveh and Ghaffarian [27] utilized a back propagation neural network to bypass high cost of frequency computations and solved such a constrained problem with enhanced colliding bodies optimization. Some studies concerned gravity dams for optimization [28]. Alimollaie and Shojaee [29] combined group method of data handling as an approximate analysis method with PSO for optimal design of a concrete arch dam under seismic excitation [29].

Although PSO is a widely used meta-heuristic for several engineering fields, it has some weak points in its standard form. Alimollaie and Shojaee [29] stated slow convergence in final iterations and capability of being trapped in local optima as deficiencies of PSO. Shahrouzi and Salehi [30] compared 8 meta-heuristic algorithms revealing that standard PSO was not as good as some others in 13 benchmark functions; however, it showed superior quality in a few test functions.

A common way to enhance searching capabilities of PSO, is to hybridize it with some other meta-heuristics [31]. In this regard, the present work develops a hybrid method

[DOI: 10.22068/ijoce.2023.13.4.564]

combining SA, ACO and PSO to achieve better performance in optimal design of dams. Shape optimization of Morrow point dam is then treated as a practical large-scale case study to evaluate enhancement of such a swarm intelligent algorithm. Full finite element analyses are employed to obtain accurate results and ensure feasibility of the optimal designs.

2. CONCEPTS AND DEVELOPMENT OF THE PROPOSED ALGORITHM

Before introducing our enhanced swarm intelligent algorithm, a basic methods are briefed here to provide the theoretical support. A vast number of optimization algorithms fall in the category of directional search [32, 33] as they apply vector-sum operations to generate new solutions from previous ones; e.g. by the following common relation:

$$X_i^t = X_i^{t-1} + V_i^t \tag{1}$$

where X_i^t x_i^t stands for the design vector of the i^{th} individual at the iteration t. The velocity vector V_i^t is the corresponding difference vector of that individual in moving from the position X_i^{t-1} to X_i^t. Different algorithms of this category have different details to calculate and update such a velocity vector.

2.1 Particle Swarm Optimizer

Particle Swarm Optimization, PSO is a very popular meta-heuristic algorithm in the category of directional search. As first introduced by [12], PSO is an attempt to simulate some actions in natural bird flocks when flying together in a swarm. The simulated flights are introduced via three terms in the following velocity vector; i.e. the inertial, the cognitive and the social terms:

$$V_i^t = c_1 V_i^{t-1} + rand \times c_2 (B_i^{t-1} - X_i^{t-1}) + rand \times c_3 (G^{t-1} - X_i^{t-1}) \tag{2}$$

The inertial term in such a vector-sum formula, denotes a vector in the direction of previous velocity vector; scaled by the factor c_1. The vector $(B_i^{t-1} - X_i^{t-1})$ is directed from the position X_i^{t-1} toward the i^{th} individual's best-experience denoted by the vector B_i^{t-1}. Such a cognitive term is further scaled by the constant factor c_2 and the function *rand* that generates random numbers between 0 and 1. Applying such a random operator improves the explorative feature of the algorithm. The third term is called social because it applies the global best experience over the whole swarm the target toward which the vector from the position X_i^{t-1} is directed. Such a vector is further scaled by the social factor c_3 and the random value *rand*. Such a vector-sum formula with random scaling is directly applicable to continuous optimization problems.

2.2 Ant Colony Optimization

Ant Colony Optimization, ACO, stands for a class of meta-heuristic algorithms inspired by

[DOI: 10.22068/ijoce.2023.13.4.564]

stigmergy between natural ants and their environment [34]. The term stigmergy refers to the indirect interaction of natural creatures with each other by changing their environment. When a natural ant walks between two stations; similarly the artificial ant goes through an edge of the corresponding graph in the computer simulation. The process continues for each ant until it completes a tour (a path graph) that represents a complete design vector; for which the objective function is evaluated.

Natural ants smell the remained amount of a chemical instance called pheromone in the forward path, to select their best way. Such a process is simulated in ACO to provide indirect sharing of experienced information between artificial search agents. An ACO algorithm may use two guiding parameters; namely attractiveness and pheromone trail. Attractiveness is a problem-specific local guide while the pheromone trail is crucial for an ACO algorithm. Its use can be generalized in the population-based algorithms provided that the characteristic graph and related paths be adequately defined. Because of applying pheromone on the edges of the graph; ACO methods are basically suited for discrete problems.

2.3 Pseudo-random Directional Search

PSO and ACO apply different strategies to solve an optimization problem. Some investigators have already utilized hybrid approaches to take merit of both [32,35]. Pseudo-random Directional Search, PDS [35] is one of them that offers a particular selection process using a bi-partite characteristic graph [36] to solve either a discrete or continuous optimization problem.

Like PSO, PDS also employs directional search via Eq. (1); however, by a different way of generating the velocity vector. It is given by:

$$V_i^t = S_j = rand \times c_j (T_j - X_i^{t-1}) \tag{3}$$

Where T_j stands for the j^{th} one among a prescribed set of state-targets; S_j denotes that state and c_j is the corresponding scale factor. Each state-target introduces a formula generating a target position; toward which the new velocity vector is oriented (form the position x_i^{t-1}). At every i^{th} iteration, selection of the index j is analogous to connecting an edge between the vertex i in the first part to the vertex j in the second part of the characteristic graph. Hence, such a bi-partite graph has the ID number of particles in its first part and the ID number of state-targets in the second; provided that each edge is limited to be drawn from the first part to the second.

Selecting a state by a particle is performed by the pheromone trail strategy. Once a state-target k is selected by the particle i an amount of pheromone (denoted by τ_{ik}) is updated on the edge *i-k*. The remained pheromone trail on these edges acts as a guide for future selection of the state. A probability value p_{ik} is calculated based on the remained pheromone on the edges *i-l* by:

[DOI: 10.22068/ijoce.2023.13.4.564]

$$p_{ik} = \frac{\tau_{ik}}{\sum_{l=1}^{N_s} \tau_{il}} \tag{4}$$

Applying a roulette-wheel lemma on p_{ik} (such as in genetic algorithms); a state index is determined as ${}_j{}^P$ among the total N_s states. At any iteration in PDS, final selection of the state j by a particle i is performed by:

$$j = \begin{cases} \arg\max_k p_{ik} & if \quad r < q_0 \\ j^R & if \quad r > q_1 \\ j^P & otherwise \end{cases} \tag{5}$$

where q_0 and q_1 are two prescribed thresholds and r is a random value between 0 and 1. The index j^P is generated as a random integer between 1 and N_s. This way, the previous experiences of state selection are indirectly shared via pheromone trails and applied either by the $\arg\max_k(.)$ function (deterministic) or via roulette wheel (stochastic) or purely random. $\arg\max_k q_k$ stands for the index that corresponds to the maximum value of q over various k's. Further details about pheromone update in PDS can be found in [35].

PSO applies the velocity of each particle by summation of inertial, cognitive and social terms in every iteration. It is while the movement of a particle in PDS, can include different states in different iterations; each one selected using indirect share of previous experiences.

2.4 Simulated Annealing

In 1980's a natural phenomenon was simulated for numerical optimization that mimics annealing process in materials; particularly some kinds of metals. The governing rule; called Boltzman machine, introduces how probable is that molecules (or atoms) of the annealed metal be re-positioned into their crystal form with the minimum state of energy during the annealing process. The probability of jumping to a higher energy state is given by:

$$P(\Delta E, T) = e^{-\frac{\Delta E}{b.T}} \tag{6}$$

in which ΔE denotes the energy difference at the temperature T , while b stands for the Boltzman coefficient. It is also called a metropolis strategy that is employed in the Simulated Annealing, SA by [9] as an optimization algorithm. Such a relation results in a higher probability of jumping in lower temperatures; that is commonly provided with the iterations of the algorithm. In perturbing a current design vector to a new candidate position, the Boltzman formula allows hill-climbing jumps even in case of increasing the cost function. Hence, it provides SA the capability of escaping from local optima toward global optimum [37]. The application of this Boltzman formula is not merely limited to such an

[DOI: 10.22068/ijoce.2023.13.4.564]

optimization algorithm; but several attempts address its hybrid applications or its use in the dynamic tuning of control parameters in another main algorithm [38–40].

2.5 The proposed hybrid optimization algorithm

PSO is a popular mete-heuristic with a high exploration feature; however, it may suffer from lack of search refinement in some cases. In this regard, one solution is parameter tuning which is case dependent and may not be easy for large-scale real world problems. Another way to improve performance of PSO is offered here by hybridizing some features from ant colony optimization and simulated annealing.

The framework of PDS is extended here for such a purpose. It not only takes merit of pheromone-based information sharing like ACO but also applies vector oriented movements such as PSO; however, the vector-sum forms during iterations of PDS. It also employs a roulette-wheel selection strategy that is widely applied in evolutionary and genetic algorithms. Consider the following relation:

$$V_i^{'} = \eta^{t-1} c_1 V_i^{t-1} + rand \times c_2 (B_i^{t-1} - X_i^{t-1}) + rand \times c_3 (G^{t-1} - X_i^{t-1}) + rand \times c_4 (X_i^R - X_i^{t-1}) \tag{7}$$

It has an extra term with respect to the velocity update relation of PSO; that is moving toward a random position within its allowable limits denoted by $X_i^R \in [X^L, X^U]$. The lower and the upper bounds on the design variables are denoted by the vectors X^L and X^U, respectively. The fourth term is inserted to improve explorative feature of the algorithm. In addition, the inertial factor is geometrically decreased by the term η^{t-1} where η is a positive constant of less than one. Such a modification provides more exploration as the iteration number t increases. Every state S_j is then generated by vanishing all factors c_k except c_j in the above velocity relation to obtain:

$$S_1 = c_1 V_i^{t-1} \tag{8}$$

$$S_2 = rand \times c_2 (B_i^{t-1} - X_i^{t-1}) \tag{9}$$

$$S_3 = rand \times c_3 (G^{t-1} - X_i^{t-1}) \tag{10}$$

$$S_4 = rand \times c_4 (X_i^R - X_i^{t-1}) \tag{11}$$

The proposed method selects each state from the set of $\{S_1,S_2,S_3,S_4\}$ using selection rule of Eq. (5). Fig. 1 demonstrates a schematic of the corresponding bi-partite graph form N_p particles to N_s states. In this regard, all the pheromone trails τ_{ik} are initiated with unity and then updated using the following relation.

$$\tau_{ik}^{\ t} = \tau_{ik}^{\ t-1} + \alpha [1 - \mu(1 - \gamma^t)] \tag{12}$$

[DOI: 10.22068/ijoce.2023.13.4.564]

where α and μ are constant factors. The term γ^t modifies the amount of pheromone deposition when the iteration t increases from 1 to $t_{\max}$. This term is controlled by a relation similar to Boltzman machine for the probability of particles' jumping as the annealing energy changes. Here, γ^t is calculated at each iteration t as follows using the Boltzman coefficient: b. Fig. 2 shows variation of γ^t with iteration t for sample values of b and $t_{\max}$.

$$\gamma^t = e^{-\frac{(t-1)}{b.t_{\max}}} \tag{13}$$

The aforementioned operators are hybridized, here, in a *Modified Particle Swarm Optimizer*, MPSO. It is introduced via the following steps:

Step 1. Initiate a population of N_p particles within variable's limits. Such a vector for every i^{th} individual can be obtained by:

$$X_i = X^L + R \otimes (X^U - X^L) \tag{14}$$

The sign $\otimes$ stands for component-wise product while R is generated as a vector of random numbers between 0 and 1. Start the particle best matrix of $[B_i^1]$ by the initial population.

Step 2. Initiate the matrix of pheromone trails $[\tau]$ by 1 with N_P rows and N_s columns ($N_s=4$). Set the iteration number as $t=1$.

Step 3. Evaluate the cost function for all individuals

Step 4. While $t < t_{\max}$ do Steps 5, 6 and 7.

Step 5. Update the global best vector as G^t and increase the iteration number t by 1.

Step 6. If $t \le \delta t_{\max}$ for every i^{th} particle do:

Generate the candidate position X_i^{Candid} by:

$$X_i^{Candid} = X_i^{t-1} + \eta^{t-1} c_1 V_i^{t-1} + rand \times c_2 (B_i^{t-1} - X_i^{t-1}) + rand \times c_3 (G^{t-1} - X_i^{t-1}) \tag{15}$$

Evaluate the candidate position and replace it with the corresponding particle in case the candidate is fitter than it.

Update the particle-best experience (cognitive position)

[DOI: 10.22068/ijoce.2023.13.4.564]

Step 7. If $t > \delta t_{\max}$ for every i^{th} particle do:

Select j and the consequent state S_j by:

$$j = \begin{cases} \arg\max_k p_{ik} & if \quad r < q_0 \\ \\ j^P & otherwise \end{cases} \tag{16}$$

Generate the candidate position by the following formula with a perturbation factor ε :

$$X_i^{Candid} = X_i^{t-1} + S_j + \varepsilon \sum_{k \neq j} S_k \tag{17}$$

Evaluate the candidate position and replace it with the corresponding particle in case the candidate is fitter than it.

Update the particle-best experience (cognitive position)

Step 8. Announce G^t as the optimum solution.

Note that the first $\delta.t_{\max}$ iterations are similar to PSO with geometric decay in the inertial term while the remainder hybridizes the prescribed operators from PSO, ACO and SA. It can also be considered an extension of PDS that applies $S_j + \varepsilon \sum_{k \neq j} S_k$ in its velocity update.

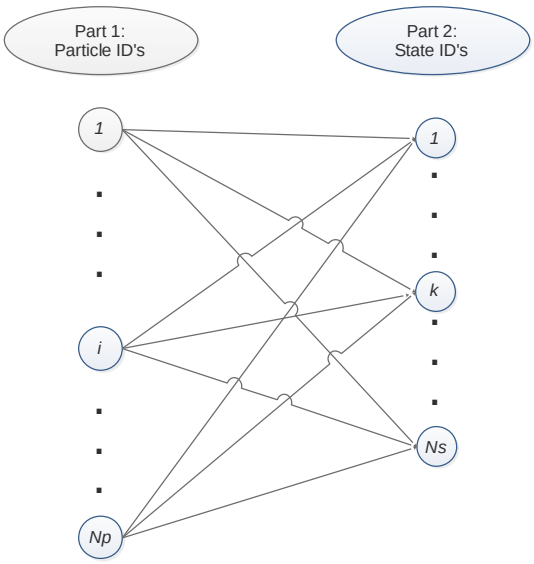

Figure 1. The characteristic bi-partite graph for state selection and pheromone deposit

[DOI: 10.22068/ijoce.2023.13.4.564]

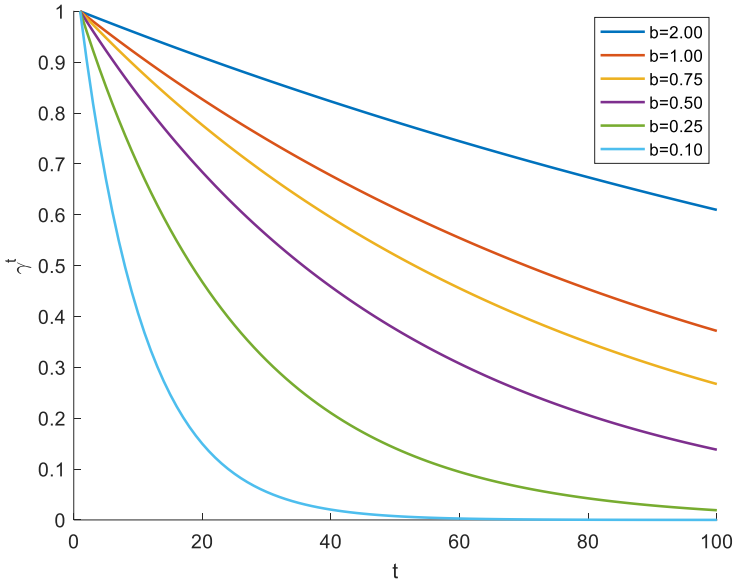

Figure 2. Sample variation of the proposed annealing function for different Boltzman's factor vs. iteration (t)

3. UNCONSTRAINED OPTIMIZATION

Performance of a new optimization algorithm can be evaluated in solving standard test functions. Such a task deals with just simple bounds on variables; practically satisfied by a fly-to-boundary technique [41,42]. For a more rigorous evaluation, the test functions of CEC2005 competition are treated. These functions; i.e. CF1 to CF6 are plotted in Fig. 3 with the definitions given in Table 1 [43]. They are solved by the proposed MPSO and PSO in comparison with a number of other meta-heuristics including LAPO [44], FOA [14], ASO [15], BES [45] and AO [16].

Table 2 gives specific control parameters of each algorithm while 20 population members and 2000 function calls are identically set for all of them. The selected algorithms cover a variety of control parameters from LAPO (with no specific parameter) to FOA with 7 and MPSO with 10 specific parameters. Each problem is solved via 30 independent trial runs preserving fair comparison conditions [17].

The statistical results are summarized in Table 3. It is observed that the proposed MPSO has approached the global optimum of CF1 by a tiny threshold in the order of $O(10^{-5})$; well superior to the best result of PSO as 0.06 and also to the others. Regarding the mean results on CF1, MPSO has obtained 0.15; that is 15 times better than PSO and 5 times smaller than 0.76 by FOA which is itself the best among the others.

[DOI: 10.22068/ijoce.2023.13.4.564]

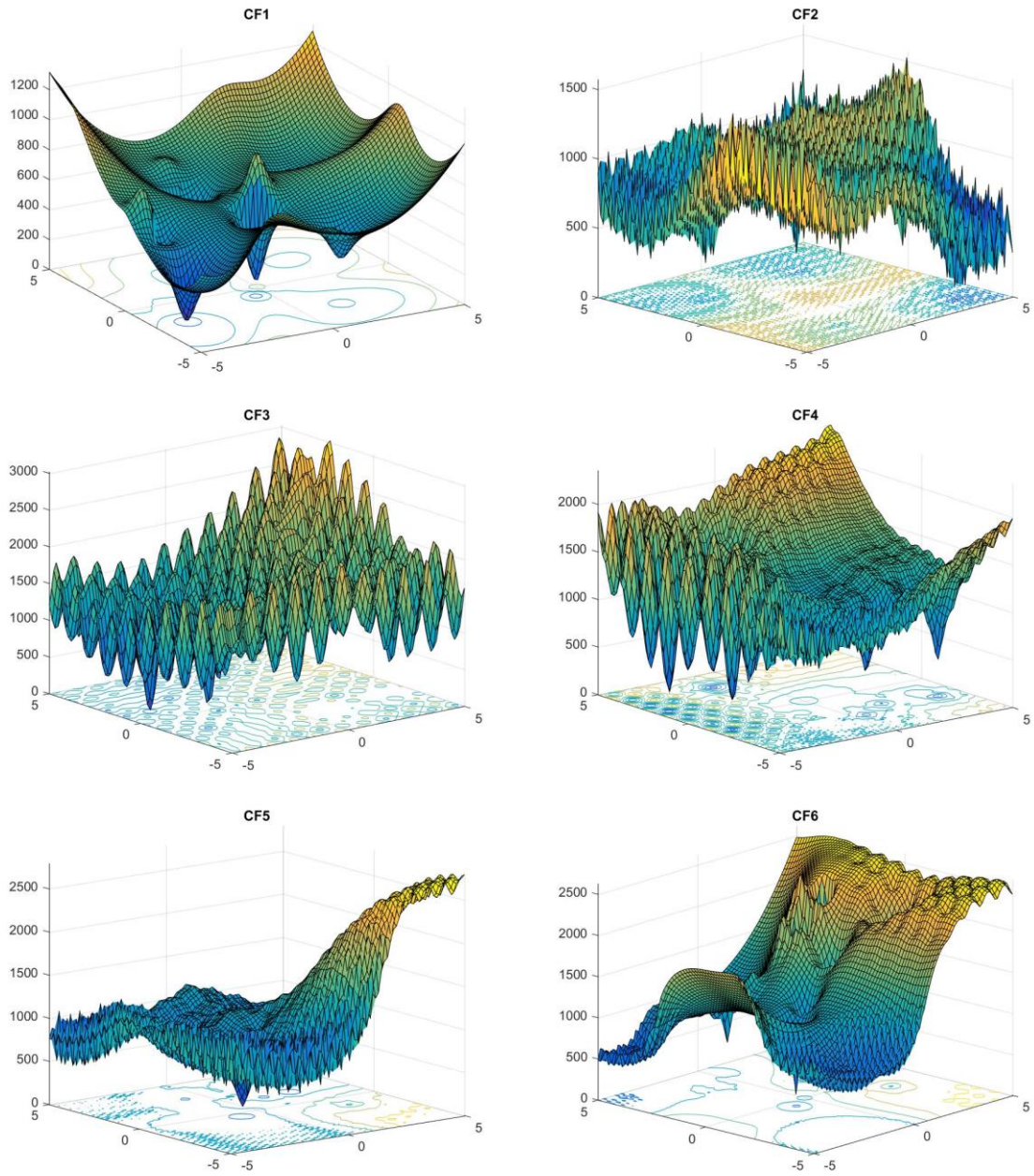

Figure 3. Composite/hybrid test functions CF1~CF6; plotted in the domain of $[-5, 5]^2$

According to Table 3, such a superiority in the best optima has remained stable in solving CF2 to CF6; particularly in comparison of MPSO with PSO. A similar trend is observed for the mean results except in solving CF3 where FOA has revealed 17.78 and MPSO has the second rank by obtaining 40.19, on average.

Table 3 also declares that in most of the treated cases, the proposed method has exhibited

[DOI: 10.22068/ijoce.2023.13.4.564]

competitive standard deviation (SD) with the other methods revealing its robustness in solving such complex test functions.

Table 1: Definition of the benchmark functions

Function	Definition	Type
CF1	$f_1, f_2, ..., f_{10} = Sphere\ function$ $\sigma_1, \sigma_2, ..., \sigma_{10} = [1,1,...,1]$ $\lambda_1, \lambda_2, ..., \lambda_{10} = [5/100, 5/100, ..., 5/100]$	composite
CF2	$f_1, f_2, ..., f_{10} = Greiwank's\ function$ $\sigma_1, \sigma_2, ..., \sigma_{10} = [1,1,...,1]$ $\lambda_1, \lambda_2, ..., \lambda_{10} = 5./[100,100,...,100]$	composite
CF3	$f_1, f_2, ..., f_{10} = Greiwank's\ function$ $\sigma_1, \sigma_2, ..., \sigma_{10} = [1,1,...,1]$ $\lambda_1, \lambda_2, ..., \lambda_{10} = [1,1,...,1]$	composite
CF4	$f_1, f_2 = Ackley's\ function \quad f_3, f_4 = Rastrigin's\ function$ $f_5, f_6 = Weierstrass\ function \quad f_7, f_8 = Greiwank's\ function$ $f_9, f_{10} = Sphere\ function$ $\sigma_1, \sigma_2, ..., \sigma_{10} = [1,1,...,1]$ $\lambda_1, \lambda_2, ..., \lambda_{10} = 5./[32,32,1,1,0.5,0.5,100,100,100,100]$	hybrid
CF5	$f_1, f_2 = Rastrigin's\ function \quad f_3, f_4 = Weierstrass\ function$ $f_5, f_6 = Greiwank's\ function \quad f_7, f_8 = Ackley's\ function$ $f_9, f_{10} = Sphere\ function$ $\sigma_1, \sigma_2, ..., \sigma_{10} = [1,1,...,1]$ $\lambda_1, \lambda_2, ..., \lambda_{10} = [0.2, 0.2, 10, 10, 0.05, 0.05, 5/32, 5/32, 0.05, 0.05]$	hybrid
CF6	$f_1, f_2 = Rastrigin's\ function \quad f_3, f_4 = Weierstrass\ function$ $f_5, f_6 = Greiwank's\ function \quad f_7, f_8 = Ackley's\ function$ $f_9, f_{10} = Sphere\ function$ $\sigma_1, \sigma_2, ..., \sigma_{10} = [0.1, 0.2, 0.3, ..., 0.9, 1]$ $\lambda_1, \lambda_2, ..., \lambda_{10} = [0.02, 0.04, 3.00, 4.00, 0.5\times0.05, 0.6\times0.05, 0.7\times5/32, 0.8\times5/32, 0.9\times0.05, 1\times0.05]$	hybrid

Nevertheless, MPSO shows considerable improvement with respect to PSO as a main objective of this experiment on unconstrained optimization. In the next part of this study, the optimal shape design of a concrete arch dam will be treated as a highly-constrained practical problem.

[DOI: 10.22068/ijoce.2023.13.4.564]

Table 2: Control parameters of the applied optimization algorithms

PSO	MPSO	LAPO	BES	FOA	ASO	AO
	$C_i = 2$			$C_c = 2.0$		
	$C_c = 2$			$C_s = 2.0$		$\alpha = 0.1$
$C_i = 1$	$C_s = 2$		$a = 10$	$f_c = 2.0$	$\alpha = 50$	$\delta = 0.1$
$C_c = 2$	$q_0 = 0.10,\ b = 0.25$	-	$R = 1.5$	$AP = 0.1$	$\beta = 0.2$	$\omega = 0.005$
$C_s = 2$	$\alpha = 0.10, \mu = 0.01,$		$\alpha = 2$	$DP = 0.8$		$u = 0.0265$
	$\delta = 0.05, \eta = 0.99$			$\alpha = 0.1$		$r_0 = 10$
	$\varepsilon = 0.01$			$b = 1.0$		

Table 3: Results comparison in optimizing test functions

Function		PSO	MPSO	LAPO	BES	FOA	ASO	AO
	Best	0.06	1.8E-05	0.03	0.07	0.03	25.66	00.12
CF1	Mean	2.33	0.15	38.30	98.29	0.76	281.79	46.00
	SD	4.38	0.78	29.93	147.31	1.34	89.26	46.96
	Best	3.84	0.13	35.96	47.27	3.55	164.94	4.25
CF2	Mean	154.15	27.93	130.25	203.47	89.54	297.44	108.01
	SD	92.53	30.37	45.76	141.78	79.38	46.54	47.42
	Best	0.66	0.01	3.22	0.62	0.27	210.91	2.93
CF3	Mean	128.11	40.19	79.86	282.91	17.78	644.45	132.51
	SD	164.24	67.39	96.73	312.19	32.25	172.57	126.41
	Best	132.71	2.64	201.73	235.15	104.35	402.57	54.63
CF4	Mean	215.31	195.98	368.35	608.99	356.73	751.81	308.85
	SD	64.05	76.41	98.21	220.26	94.36	160.50	157.75
	Best	0.63	0.003	0.34	1.03	0.95	107.94	0.40
CF5	Mean	111.17	36.91	74.65	223.46	69.41	538.22	38.06
	SD	147.70	48.84	44.53	261.65	47.64	163.01	46.65
	Best	105.03	100.03	107.98	174.31	110.78	314.08	124.06
CF6	Mean	409.29	229.28	349.28	409.35	377.91	475.18	373.60
	SD	119.23	155.12	110.52	104.24	118.94	32.43	103.13

4. GEOMETRY ASSESSMENT OF THE DOUBLE-CURVED DAMS

Arch dams are structures that rely on the spatial form of their body to withstand the applied

[DOI: 10.22068/ijoce.2023.13.4.564]

loads. Horizontal and vertical profiles in a concrete dam as well as the corresponding dimensions have a major role in providing sufficient stability and structural strength [2]. In the other hand, the cost of the construction material; i.e. concrete, is so high that makes it reasonable to seek for its minimal value under the given constraints. The optimal dam-geometry is also affected by the material strength and the shape of the valley surrounding the dam [46].

When a designer attempts to determine the geometrical shape of a double-curved dam, the crown cantilever is concerned first and then the horizontal rings should be determined at all vertical levels. However in an automatic optimal design procedure, both vertical and horizontal design parameters can simultaneously be altered until their optimal values are found. Such parameters commonly obey some template shapes to govern the geometry of a double-curved dam. The template relations have already been offered and upgraded by a number of investigators [2,7]. Prior to formulating the optimization problem we describe the applied template relations and their parameters to asses shape of the double-curved dam.

4.1 Geometric description of crown cantilever

According to Fig. 4, shape of the crown cantilever (the vertical profile) depends on the upstream and downstream curves. Once the upstream curve and local thicknesses are derived, the central curve can be configured. A third-order polynomial function [47] is used to define the up-stream curve in the center-line of the dam:

$$y(z) = -S_1 z + \frac{S_1 - \beta^2 (S_1 + S_2)}{2\beta h(1-\beta)} z^2 - \frac{S_1 - \beta(S_1 + S_2)}{3\beta h^2 (1-\beta)} z^3 \tag{18}$$

whereas h, S_1 and S_2 are the height of the dam, slope in the crown and slope in the footing, respectively. A fraction of the dam height which corresponds to zero slope is denoted by $z = \beta h$.

Suppose the dam height is discretized by n parts (at $n+1$ levels). Consequently, thickness of the crown cantilever is interpolated from thickness at $n+1$ levels as:

$$t_C(z) = \sum_{i=1}^{n+1} L_i(z) \times t_{Ci} \tag{19}$$

At any i^{th} level, t_{c_i} stands for the crown cantilever thickness while $L_i(z)$ denote the corresponding Lagrange interpolator function; given by:

$$L_i(z) = \frac{\prod_{m=1}^{n+1} (z - z_m)}{\prod_{i=1}^{n+1} (z_i - z_m)} \quad m \neq i \tag{20}$$

where z_i and z_m stand for the coordinates at the i^{th} and m^{th} levels of the central cantilever, respectively. In the present study, the number of subdivided parts n is taken 5. Consequently,

[DOI: 10.22068/ijoce.2023.13.4.564]

n+1 corresponding height levels are denoted by $z_i = \lambda_i h$ where the counter index *i* can be an integer between 1 and 6.

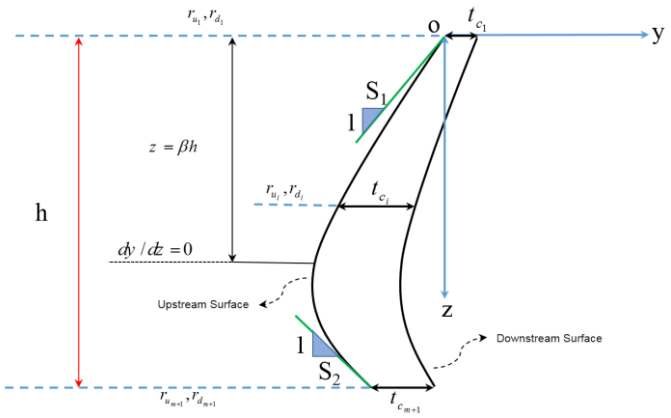

Figure 4. Shape of a typical double-curved dam and the governing variables

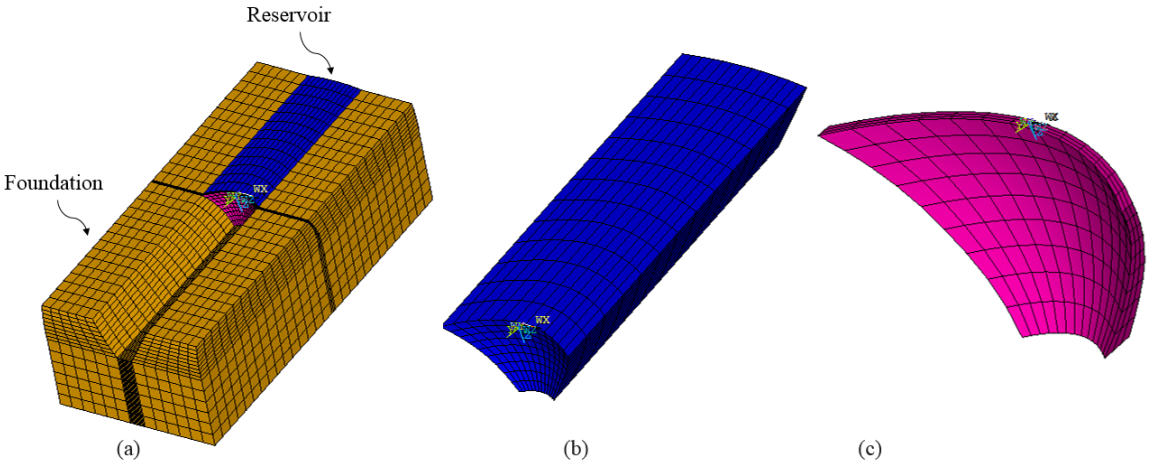

Figure 5. Finite element model of Morrow Point dam: (a) Integrated dam_water_foundation rock system, (b) dam-lake system, (c) dam body

4.2 Geometric description of the central horizontal arch ring

A typical profile of the dam body is depicted in Fig. 4. It is distinguished by the second-order functions defining the upstream and downstream curves as recommended in the literature [7]. The corresponding relations are given as:

$$y_{cu}(x,z) = \frac{1}{2r_u(z)}x^2 + B(z) \tag{21}$$

[DOI: 10.22068/ijoce.2023.13.4.564]

$$y_{cd}\left(x,z\right)=\frac{1}{2r_d\left(z\right)}x^2+B\left(z\right)+t_c\left(z\right) \tag{22}$$

r_d and y_{cd} denote the radius and y-coordinate of the downstream curve, respectively. The interpolated function $B(z)=y(z)$. The corresponding values for the upstream curve are given as r_u and y_{cu}. Height-wise variation of such radii are obtained by Lagrange interpolation as follows:

$$r_u\left(z\right)=\sum_{i=1}^{n+1}L_i(Z)\times r_{u_i} \tag{23}$$

$$r_d\left(z\right)=\sum_{i=1}^{n+1}L_i(Z)\times r_{d_i} \tag{24}$$

This way, the horizontal and vertical shape of the dam is determined based on the thickness, upstream and downstream radii at $n+1=6$ equal-distant points. Due to real-world conditions in construction of the dam, its plan section may be inclined about the central z-axis by the angle φ.

4. PROBLEM FORMULATION

It is aimed to minimize total concrete volume V in the body of the double-curved dam by altering its shape so that it can withstand the design loads.

$$\min\ V(X)=\sum_{e=1}^{N_e}v_e \tag{25}$$

The volume of every e^{th} element is denoted by v_e. According to the previous relations, the design vector X for shape optimization of the double-curved dam is defined as:

$$X=\left\{t_{c1},...,t_{c6},r_1,...,r_6,R_1,...,R_6,S_1,S_2,\beta,\phi\right\}^T \tag{26}$$

Such a design vector has 22 continuous variables. The constraints in such an optimization problem are denoted by side limits $X^L\le X\le X^U$ and behavior constraints in the general form of $g_m(X)\le 0$ for any m^{th} constraint. During the optimization, the design variables are enforced to fall within their side bounds; however, satisfaction of the other constraints are ensured by an external penalty approach to provide required stability and serviceability. The problem formulation is transformed into fitness maximization as:

[DOI: 10.22068/ijoce.2023.13.4.564]

$$\max\ Fitness(X) = -\zeta(X) = -V(X) \times [1 + k_p \sum_m \max(0, g_m(X))] \tag{27}$$

The penalized cost is denoted by $\zeta(X)$ as reverse of the fitness function. The penalty factor k_p is selected large enough to achieve feasible optimal designs by MPSO. In this problem, the constraints (other than simple bounds) are distinguished in stress, stability and geometrical groups [7] and are detailed as follows.

Arch dams can be constructed using mass concrete without any reinforcement. The design, safe operation and stability of the structure are controlled based on the allowable stress method. The maximal absolute stresses are computed by finite element analysis after generating the dam shape and its structural model. Such stresses are subject to the following constraints:

$$G_1(X) = \frac{\sigma_c}{F_c} - 1 \le 0 \tag{28}$$

$$G_2(X) = \frac{\sigma_t}{F_t} - 1 \le 0 \tag{29}$$

σ and F represent the principal stress and allowable uniaxial strength, respectively. The subscript *t* stands for tension while *c* stands for compression.

To provide stability, the central ring angle of the arch dam is controlled here at various height levels by:

$$G_{3,i}(X) = \frac{\varphi_i}{\varphi^U} - 1 \le 0 \tag{30}$$

$$G_{4,i}(X) = 1 - \frac{\varphi_i}{\varphi^L} \le 0 \tag{31}$$

in which φ^L and φ^U represent the minimum and maximum allowable central angle and φ_i is the angle at the i^{th} height level.

Geometrical constraints are applied due to executive considerations during the construction phase. In this study, three geometrical constraints are considered: overhang and undercut slopes, upstream and downstream radii and dam thickness among its height.

Crown cantilever curve slopes at the overhang and undercut levels are defined as partial geometrical constraints. s_1 and s_2 denote the overhang and undercut slopes, respectively. They are confined to their allowable limit: s_{all} by the following relations.

[DOI: 10.22068/ijoce.2023.13.4.564]

$$G_5(X) = \frac{S_1}{S_{all}} - 1 \le 0 \tag{32}$$

$$G_6(X) = \frac{S_2}{S_{all}} - 1 \le 0 \tag{33}$$

Table 4: Mechanical properties for materials of the dam-water-rock system

Parameter	Value (Unit)
Dam-body Concrete	
Mass Density	2483 (Kg/m^3)
Elasticity modulus	27580 (MPa)
Poisson's Ratio	0.20
Uniaxial compressive strength	30 (MPa)
Uniaxial tensile strength	1.5 (MPa)
Water	
Mass Density	1000 (Kg/m^3)
Velocity of Pressure Waves	1440 (m/s)
Wave reflection coefficient	0.90
Foundation rock Properties	
Mass Density	2483 (Kg/m^3)
Elasticity modulus	27580 (MPa)
Poisson's Ratio	0.25

To prevent the coincidence of the upstream and downstream curves, the following constraint is applied:

$$G_{7,i}(X) = \frac{r_i}{R_i} - 1 \le 0 \tag{34}$$

in which, r_{d_i} and r_{u_i} denote the radii of the downstream and upstream curves at the i^{th} interpolation point, respectively.

Due to construction and gravitational load considerations, the thickness of each point among the dam height should not be greater than a neighbor point above it. This geometrical constraint is thus applied by the following relation:

$$G_{8,i}(X) = \frac{t_{c,i}}{t_{c,i+1}} - 1 \le 0 \tag{35}$$

where $t_{c,i}$ stands for the thickness of the dam in the crown vertical for the i^{th} height level.

[DOI: 10.22068/ijoce.2023.13.4.564]

Table 5: Lower and upper bounds on the design variables

Variable	X^L	X^U
$t_{c,1}$	7	10
$t_{c,2}$	8	15
$t_{c,3}$	12	20
$t_{c,4}$	15	25
$t_{c,5}$	17	30
$t_{c,6}$	20	35
$r_{d,1}$	115	156
$r_{d,2}$	99	133
$r_{d,3}$	82	111
$r_{d,4}$	65	88
$r_{d,5}$	48	65
$r_{d,6}$	31	42
$r_{u,1}$	115	156
$r_{u,2}$	99	133
$r_{u,3}$	82	111
$r_{u,4}$	65	88
$r_{u,5}$	48	65
$r_{u,6}$	31	42
s_1	0.09	0.36
s_2	0.09	0.36
β	0.5	0.9
$\varphi(^o)$	-1	1

5. SHAPE OPTIMIZATION OF MORROW POINT ARCH DAM

Morrow Point double-curvature arch dam, was constructed in 1968 over the Gunnison River, 263 km south-west of Denver in Colorado. Since then, several research works have already addressed design of this dam as a case study [48–50]. Table 4 gives the properties of the construction and environmental materials; i.e. body, water and foundation-rock [51,52]. Simple bounds on the design variables are given in Table 5.

[DOI: 10.22068/ijoce.2023.13.4.564]

Table 6: Comparison of shape designs for Morrow Point dam by different methods

Variable	USBR	PSO	MPSO
$t_{c,1}$	6.60	7.00	7.02
$t_{c,2}$	10.00	10.35	9.86
$t_{c,3}$	13.30	14.04	12.02
$t_{c,4}$	16.00	16.20	15.03
$t_{c,5}$	18.60	19.85	17.02
$t_{c,6}$	21.70	22.03	20.10
$r_{d,1}$	287.00	124.95	134.41
$r_{d,2}$	187.00	116.07	120.97
$r_{d,3}$	106.00	106.74	108.98
$r_{d,4}$	94.00	88.00	87.86
$r_{d,5}$	79.60	65.00	64.86
$r_{d,6}$	63.70	42.00	41.61
$r_{u,1}$	122.00	124.39	123.54
$r_{u,2}$	108.00	113.37	117.36
$r_{u,3}$	93.00	105.48	108.19
$r_{u,4}$	78.00	88.00	87.74
$r_{u,5}$	61.00	62.71	64.79
$r_{u,6}$	42.00	41.33	41.42
s_1	0.36	0.34	0.36
s_2	0.10	0.10	0.09
β	0.70	0.63	0.73
$\varphi(^o)$	0.00	-0.23	0.98
Best $V(m^3)$	294841.00	278236.60	233065.38
Mean V	-	263238.29	261359.51
Mean Penalized V	-	255765.40	245814.40
SD	-	16010.56	36246.26

Parts of the finite element model for the system of dam-water-rock are illustrated in Fig. 5. Such an interacting system is simultaneously modeled in three dimensions using ANSYS software [53] with the capability of automatic mesh generation. It is linked with our optimization programs in MATLAB environment [54]. During optimization, each design

[DOI: 10.22068/ijoce.2023.13.4.564]

vector is decoded to reveal the corresponding shape of the dam body. Consequently, the entire finite element model is constructed and analyzed to derive structural responses. Critical responses such as principal stresses and reactions are used to evaluate the constraints and fitness function for the corresponding design vector.

As PSO and MSPO are both stochastic methods, they are run for 60 independent trials to obtain reliable results. The problem is solved with 40 individuals up to 250 iterations while other control parameters are given in Table 2. Henceforth, 10000 finite element analyses are implemented at each run to ensure convergence of the algorithms. As such a real-world design task is computationally expensive, it is highly rewarding to improve efficiency and effectiveness of PSO via the proposed MPSO.

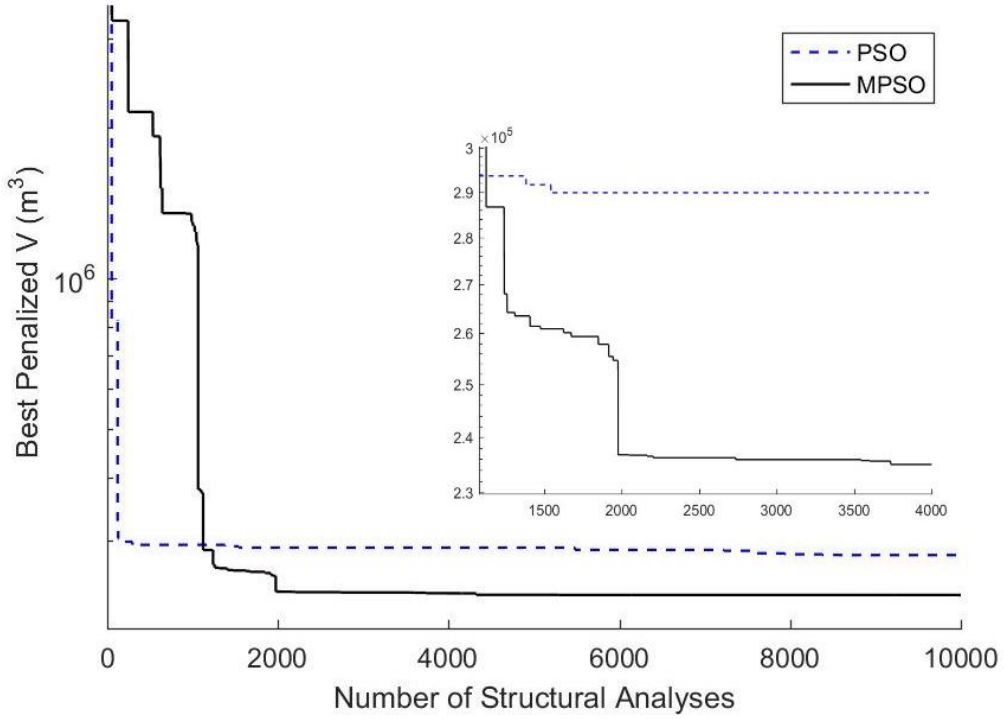

Figure 6. Convergence comparison for the best run of MPSO vs. PSO in shape optimization of Morrow Point dam

In order to evaluate design improvement via optimization with respect to common practice, the Morrow Point dam is once designed by the procedure of USBR and Varshney's method [55,56]. Such a single practical design is then inserted in the initial population of particles that are randomly generated during optimization. The initial population is identically used for each independent run of PSO and MPSO to provide a fair comparison between them; however, it is regenerated in every new run.

[DOI: 10.22068/ijoce.2023.13.4.564]

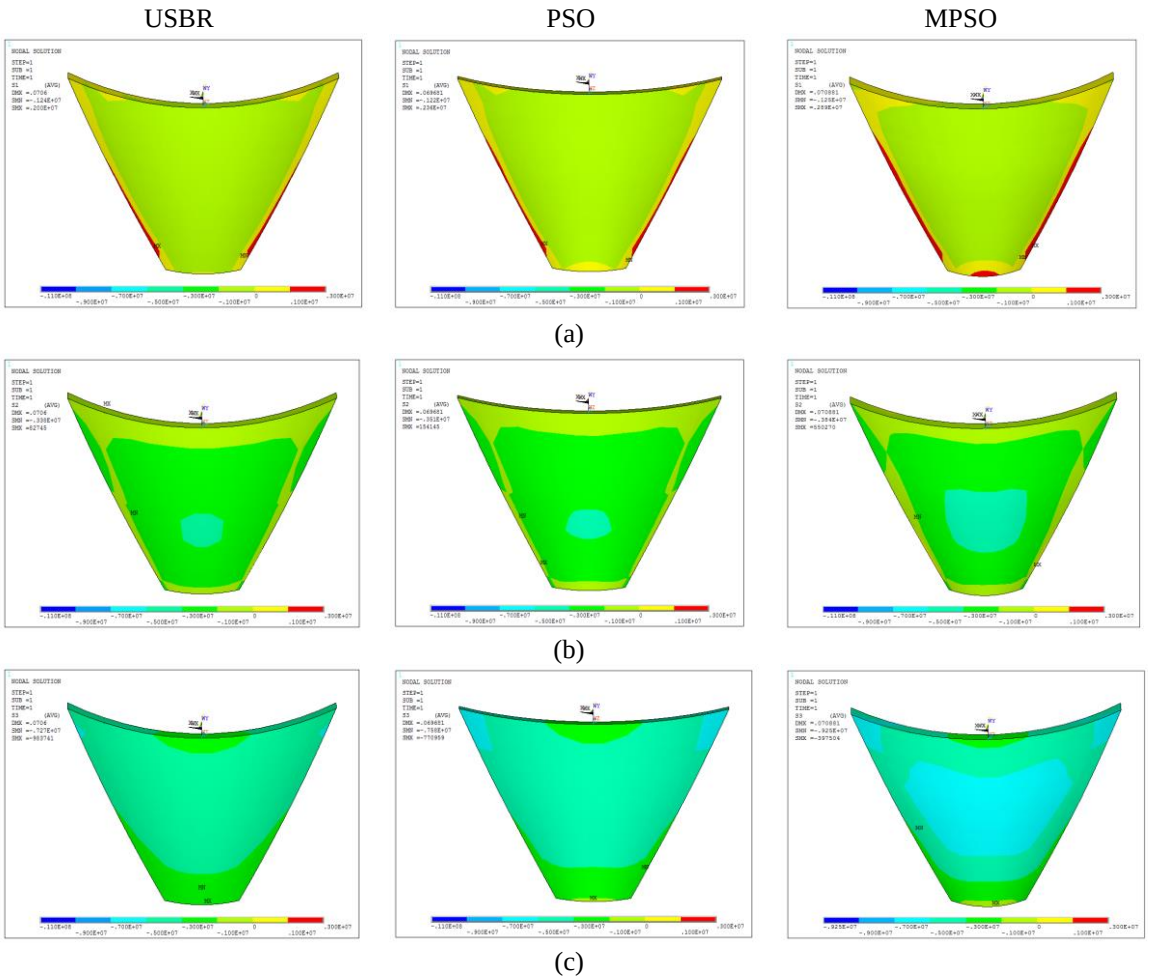

Figure 7. Comparison of principal stresses in final design of Morrow Point dam by USBR vs. optimal designs by PSO and MPSO: (a) σ_1 ,(b) σ_2 and (c) σ_3

During this numerical experiment no feasible optimal design coincided with the design by USBR's method; i.e. structural volume of 294841.0 m^3 for the concrete in the dam body. The mater indicates that such a practical design is not optimal. According to Table 6, the best design of PSO resulted in a volume of 278236.6 m^3 which is 6% lower than USBR's design. MPSO exhibits more improvement of 21% in obtaining its best design that weighs 233065.4 m^3. In another word, the proposed MPSO has considerably reduced the material consumption by 61776 m^3 with respect to the common practice (USBR) and 45171 m^3 with respect to PSO. Fig. 6 reveals superior convergence of MPSO with respect to PSO in such an optimization run. It is observed that PSO has revealed a rapid initial drop in the penalized cost; however, it has further been ended with a less-fit local optimum. In contrary, the proposed MPSO has exhibited better search refinement than PSO and has overpassed local optimum toward a fitter (lower cost) optimal design.

[DOI: 10.22068/ijoce.2023.13.4.564]

The constraints are checked and reported in Table 7 for the best designs of PSO and MPSO in shape optimization of Morrow Point dam. It can be noticed that despite PSO, the proposed MPSO has successfully satisfied all the constraints to obtain a perfect feasible design. It is while the best design of PSO has infeasibility in the stability constraint $G_{4,3}(X)$; that corresponds to an out-of-bound value for the central ring angle at the 3rd control point.

Table 6 also shows superiority of MPSO over PSO in obtaining better mean penalized cost and mean volume. The proposed MPSO has enhanced performance with respect to PSO; not only in the best design but also in constraint handling to obtain fitter mean results. According to Table 6, more standard deviation can be observed over different trails of MPSO with respect to PSO. It can indicate higher diversity maintained by MPSO during such a shape optimization.

In order to have further engineering insight on the aforementioned designs of Morrow point dam; distribution of principal stresses are compared in Fig. 7. It is observed that despite the USBR design, the optimal designs have generally distributed less stresses even in less effective parts of the dam body.

According to Fig. 7, several stress zones can be distinguished for the dam body mainly in the upstream and downstream surfaces. The tensile zone area is as small as nearly 5% of the dam surface by USBR procedure due to applying high safety factor for tension. In the best design by PSO, two narrow bands of tension stresses are detected at left and right abutments. Finally in MPSO design, tracing tension stress in the upstream surface, three high-stress narrow bands are declared at the right and left abutments and also at the bottom of the dam body. Comparison of the results indicates that the proposed optimum design has been more successful in achieving tensile capacity of the concrete dam body in the allowable range.

6. CONCLUSION

Shape optimization is treated as a crucial issue in the design of arch dams. It was formulated using 22 continuous design variables and a rigorous set of behavior constraints. A preliminary procedure of USBR as well as two swarm intelligent algorithms: PSO and MPSO were employed for the shape design of concrete double-curved dams. The proposed MPSO indirectly utilizes previous experiences of the artificial search agents via pheromone trails selecting new states to increase effectiveness of the optimization algorithm. It takes advantage of Boltzmann machine to tune the algorithm for better performance.

Performance of the proposed method was evaluated in comparison with a number of meta-heuristics in optimizing six composite test functions. Consequently, MPSO showed superior performance to PSO not only in the best but also in the mean results. In most cases, the achieved standard deviation by MPSO remained in the same range as the other treated methods revealing its competitive performance.

In shape optimization of the Morrow Point dam, it was observed that PSO and MPSO can reveal significantly lower costs than USBR design procedure. However, the optimum design of PSO had some degree of infeasibility. In contrary, the proposed MPSO was found superior to the others not only in the quality of the best final design but also in the mean

[DOI: 10.22068/ijoce.2023.13.4.564]

fitness over 60 independent runs of such an expensive task. The best result of MPSO was perfectly feasible and it provided 21% lower material cost than USBR and 16% lower than PSO. It is important from practical point of view; considering necessity of satisfying several behavior constraints and that total cost of the arch dam majorly depends on its concrete volume.

Comparison of the designs obtained by the treated methods in view of stress distributions in the dam body, revealed further superiority of the proposed hybrid algorithm over the others. The results of this study declare that principal tensile stress at the abutment of the upstream face in MPSO is greater than PSO. In conclusion, the proposed hybrid method is capable of revealing satisfactory enhancement over the well-known PSO and superior results in compared with the common practice of USBR design procedure for the arch dams.

REFERENCES

1. Yao T, Choi KK. Shape Optimal Design of an Arch Dam. *J Struct Eng* 1989;**115**:2401–5.
2. Akbari J, Ahmadi MT, Moharrami H. Advances in concrete arch dams shape optimization. *Appl Math Model* 2011;**35**:3316–33.
3. Pourbakhshian S, Ghaemian M, Joghataie A. Shape optimization of concrete arch dams considering stage construction. *Sci Iran* 2016;**23**:21–35.
4. Sharma R. *Optimal Configuration of Arch Dams*. Indian Institute of Technology, Kanpur., 1983.
5. Sharpe R. The optimum design of arch dams. *Proc. ICE - Civ. Eng.*, 1969; 73-98.
6. Wassermann K. Three-Dimensional Shape Optimization of Arch Dams with Prescribed Shape Functions. *J Struct Mech* 1983;**11**:465–89.
7. Zhu BB, Rao B, Jia J, Li Y. Shape Optimization of Arch Dams for Static And Dynamic Loads. *J Struct Eng* 1992;**118**:2996–3015.
8. Dorigo M, Stützle T. Ant colony optimization. London, UK: The MIT press; 2016.
9. Kirkpatrick S, Gelatt CD, Vecchi MP. Optimization by Simulated Annealing. *Sience* 1983;**220**:671–80.
10. Geem ZW, Kim JH, Loganathan G V. A New Heuristic Optimization Algorithm: Harmony Search. *Simulation* 2001;**76**:60–8.
11. Holland JH. *Adaptation in Natural and Artificial Systems*. University of Michigan Press; 1998.
12. Kennedy J, Eberhart R. Particle swarm optimization. IEEE Int. Conf. Part. swarm Optim., 1995; **4**:1942–8.
13. Kaveh A, Bakhshpoori T. Water Evaporation Optimization: A novel physically inspired optimization algorithm. *Comput Struct* 2016;**167**:69–85.
14. Hochsteiner E, Mariani VC, Coelho L dos S. Design of heat exchangers using Falcon Optimization Algorithm. *Appl Therm Eng* 2019;**156**:119–44.

[DOI: 10.22068/ijoce.2023.13.4.564]

15. Zhao W, Wang L, Zhang Z. Atom search optimization and its application to solve a hydrogeologic parameter estimation problem. *Knowledge-Based Syst* 2019;**163**:283–304.
16. Abualigah L, Yousri D, Abd Elaziz M, Ewees AA, Al-qaness MAA, Gandomi AH. Aquila Optimizer: A novel meta-heuristic optimization algorithm. *Comput Ind Eng* 2021;**157**:107250.
17. Shahrouzi M, Kaveh A. An efficient derivative-free optimization algorithm inspired by avian life-saving manoeuvres. *J Comput Sci* 2022;**57**:101483.
18. Zhao W, Wang L, Mirjalili S. Artificial hummingbird algorithm: A new bio-inspired optimizer with its engineering applications. *Comput Methods Appl Mech Eng* 2022;**388**:114194.
19. Rana S, Jasola S, Kumar R. A review on particle swarm optimization algorithms and their applications to data clustering. *Artif Intell Rev* 2011;**35**:211–22.
20. Liu H, Cai Z, Wang Y. Hybridizing particle swarm optimization with differential evolution for constrained numerical and engineering optimization. A*ppl Soft Comput J* 2010;**10**:629–40.
21. Storn R, Price K. Differential Evolution – A Simple and Efficient Heuristic for global Optimization over Continuous Spaces. *J Glob Optim* 1997;**11**:341–59.
22. Hadidi A, Kaveh A, Farahmand Azar B, Talatahari S, Farahmandpour C. An Efficient Hybrid Algorithm Based On Particle Swarm and Simulated Annealing for Optimal Design Of Space Trusses. *Int J Optim Civ Eng* 2011;**1**:377–95.
23. Hassani Z, Alambardar Meybodi M. Hybrid Particle Swarm Optimization with Ant-Lion Optimization: Experimental in Benchmarks and Applications. *J AI Data Min* 2021;**9**:583–95.
24. Mirjalili S-A. The ant lion optimizer. *Adv Eng Softw* 2015;**83**:80–98.
25. Parmee I-C. Genetic Algorithms and Hydropower System Design. *Comput Aided Civ Infrastruct Eng* 1998;**13**:31–41.
26. Maheri MR, Taleb-beydokhti N, Ahadi S. Shape optimization of concrete arch dams using simple genetic algorithm. *Dam Eng* 2003;**XIV**:105–40.
27. Kaveh A, Ghaffarian R. Shape optimization of arch dams with frequency constraints by enhanced charged system search algorithm and neural network. *Int J Civ Eng* 2015;**13**:102-11.
28. Kaveh A, Zakian P. Stability Based Optimum Design of Concrete Gravity. *Int J Optim Civ Eng* 2015;**5**:419–31.
29. Alimollaie S, Shojaee S. Optimal Design of Arch Dams By Combining Particle Swarm Optimization and Group Method of Data Handling. *Int J Optim Civ Eng* 2017;**7**:493–514.
30. Shahrouzi M, Salehi A. Imperialist Competitve Learner-Based Optimization: a hybrid method to solve engineering problems. *Int J Optim Civ Eng* 2020;**10**:155–80.
31. Liu M. Progressive collapse design of seismic steel frames using structural optimization. *J Constr Steel Res* 2011;**67**:322–32.

[DOI: 10.22068/ijoce.2023.13.4.564]

32. Shahrouzi M, Pashaei M. Stochastic Directional Search : an efficient heuristic for structural optimization of building frames. *Sci Iran* 2013;**20**:1124–32.
33. Yang XS. Nature-inspired optimization algorithms: Challenges and open problems. *J Comput Sci* 2020;**46**:101104.
34. Dorigo M, Birattari M. and Stutzle T. Ant colony optimization. *IEEE Comput Intel Mag* 2006; **1**(4):28-39.
35. Shahrouzi M. Pseudo-random Directional Search: a new heuristic for optimization. *Int J Optim Civ Eng* 2011;**1**:341–55.
36. Kaveh A. *Structural Mechanics: Graph and Matrix Methods.* 3rd ed. Hertfordshite, UK: Research Studies Press Ltd.; 2004.
37. Suman B, Kumar P. A survey of simulated annealing as a tool for single and multiobjective optimization. *J Oper Res Soc* 2006; **57**:1143–60.
38. Kaveh A, Shahrouzi M. Simulated annealing and adpative dynamic variable band mutation for structural optimization by genetic algorithms. *Asian J Civ Eng* 2006;**7**:651–70.
39. Ghorbani A, Akbari Jokar MR. A hybrid imperialist competitive-simulated annealing algorithm for a multisource multi-product location-routing-inventory problem. *Comput Ind Eng* 2016; **101**: 116-127.
40. Kumar S, Tejani GG, Pholdee N, Bureerat S. Improved metaheuristics through migration-based search and an acceptance probability for truss optimization. *Asian J Civ Eng* 2020;**21**:1217–37.
41. Kaveh A, Talatahari S. Hybrid charged system search and particle swarm optimization for engineering design problems. *Eng Comput* 2011;**28**:423–40.
42. Shahrouzi M, Aghabaglou M, Rafiee F. Observer-teacher-learner-based optimization: An enhanced meta-heuristic for structural sizing design. *Struct Eng Mech* 2017;**62**:537–50.
43. Liang JJ, Suganthan PN, Deb K. Novel composition test functions algorithm for numerical optimization. *IEEE Swarm Intell. Symp.* SIS'05, 2005; 68–75.
44. Nematollahi AF, Rahiminejad A, Vahidi B. A novel physical based meta-heuristic optimization method known as Lightning Attachment Procedure Optimization. *Appl Soft Comput J* 2017;**59**:596–621.
45. Alsattar HA, Zaidan AA, Zaidan BB. Novel meta-heuristic bald eagle search optimisation algorithm. *Artif Intell Rev* 2020;**53**:2237–64.
46. Mostafaei H, Sohrabi Gilani M, Ghaemian M. Stability analysis of arch dam abutments due to seismic loading. *Sci Iran* 2017;**24**:467–75.
47. Saber Mahani A, Shojaee S, Salajegheh E, Khatibinia M. Hybridizing two-stage meta-heuristic optimization model with weighted least squares support vector machine for optimal shape of double-arch dams. *Appl Soft Comput J* 2015;**27**:205–18.
48. Duron ZH, Hall JF. Experimental and finite element studies of the forced vibration response of morrow point dam. *Earthq Eng Struct Dyn* 1988;**16**:1021–39.

[DOI: 10.22068/ijoce.2023.13.4.564]

49. Salajegheh J, Salajegheh E, Seyedpoor SM, Gholizadeh S. Arch dam optimization considering fluid-structure interaction with frequency constraints using artificial intelligence methods. *14th World Conf. Earthq. Eng.*, Beijing: 2008, 1–10.
50. Talatahari S, Aalami MT, Parsiavash R. Optimum Design of Double Curvature Arch Dams Using A Quick Hybrid Charged System Search Algorithm. *Int J Optim Civ Eng* 2016;**6**:227–43.
51. USACE. *Earthquake Design and Evaluation of Concrete Hydraulic Structures*. Washington DC: US Army Corps Of Engineers; 2007.
52. Chopra AK. *Earthquake Engineering for Conceret Dams.* New Jersey, USA: John Wiley & Sons, Inc.; 2020.
53. ANSYS. ANSYS advanced analysis techniques guide. *Ansys Help* 2007:724–46.
54. MathWorks. *MATLAB, The language of technical programming* 2006.
55. Varshney RS. *Concrete Dams*. Oxford & IBH publishing company; 1982.
56. USBR. D*esign of Arch Dams: Design manual for Concrete Arch Dams*. Denver, Colorado: United States Bureau of Reclamation; 1977.

[DOI: 10.22068/ijoce.2023.13.4.564]